Earthquakes and Structures, *Vol. 15, No. 5 (2018) 487-498*
DOI: https://doi.org/10.12989/eas.2018.15.5.487

Probabilistic seismic assessment of mega buckling-restrained braced frames under near-fault ground motions

Sajad Veismoradi[1a] and Ehsan Darvishan[*2]

[1]*School of Civil Engineering, Iran University of Science & Technology, Tehran, Iran*
[2]*Young Researchers and Elites Club, Roudehen Branch, Islamic Azad University, Roudehen, Iran*

(Received May 12, 2017, Revised July 19, 2018, Accepted September 5, 2018)

Abstract. Buckling-restrained braces are passive control devices with high level of energy dissipation ability. However, they suffer from low post-yield stiffness which makes them vulnerable to severe ground motions, especially near-field earthquakes. Among the several methods proposed to improve resistance of BRB frames, mega-brace configuration can be a solution to increase frame lateral strength and stiffness and improve distribution of forces to prevent large displacement in braces. Due to the limited number of research regarding the performance of such systems, the current paper aims to assess seismic performance of BRB frames with mega-bracing arrangement under near-field earthquakes via a detailed probabilistic framework. For this purpose, a group of multi-story mega-BRB frames were modelled by OpenSEES software platform. In the first part of the paper, simplified procedures including nonlinear pushover and Incremental Dynamic Analysis were conducted for performance evaluation. Two groups of near-fault seismic ground motions (Non-pulse and Pulse-like records) were considered for analyses to take into account the effects of record-to-record uncertainties, as well as forward directivity on the results. In the second part, seismic reliability analyses are conducted in the context of performance based earthquake engineering. Two widely-known EDP-based and IM-based probabilistic frameworks are employed to estimate collapse potential of the structures. Results show that all the structures can successfully tolerate near-field earthquakes with a high level of confidence level. Therefore, mega-bracing configuration can be an effective alternative to conventional BRB bracing to withstand near-field earthquakes.

Keywords: buckling restrained braces; mega-bracing; probabilistic assessment; near-fault records; fragility assessment; pushover analysis

1. Introduction

It has been recognized by researchers that seismic ground motions close to an active fault could be extremely different than far-field ground motion records and could demonstrate unusual spectral shape, as well as large amplitude and different energy content. In near-fault zones, due to the short distance between the rupture fault and building site, high-frequency damping is minimal and so their records include high-frequency contents (Stewart *et al*. 2002). However, the most prominent characteristics of the near-fault earthquake could be devoted to the predominant velocity pulse, which can be emerged from either forward directivity or fling step effects. Forward directivity appears when the surface rupture extends toward the site, while fling step is the result of permanent ground displacement due to tectonic deformation (Kalkan and Kunnath 2006). Increasing the effects of higher modes on structures, as well as higher ductility demands and thus increasing the probability of failure are some of the influence of pulse-like near-fault ground motion which has been investigated by various research studies on different structural systems. Soleimani Amiri *et al*. (2013) studied the seismic performance of steel moment frames by pushover and nonlinear time-history analyses with forward directivity effects. Their results highlighted that various lateral load patterns in pushover cannot cover the near-fault time-history result needs. Eskandari *et al*. (2017) compared the seismic performance of reinforced concrete steel braced frames against far field and near-fault seismic records and witnessed more result dispersions of NF records for the intermediate and high-rise frames. Kalkan and Kunnath (2006) studied the pulse-like characteristics of the near-fault ground motions against far-field ground motions on the SMRFs and demonstrated that for pulse-type seismic input, the maximum demand of the frame is a function of the ratio of the pulse period to the fundamental period of the structure. Mortezaei *et al*. (2010) pinpointed the vulnerability of existing RC buildings during pulse-like ground motions and compared their structural performance against FRP-strengthened RC buildings.

As can be noted from previous researches, the use of structural systems with high ductility and effective seismic energy absorbing for the active near-fault zones is inevitable. Therefore, many different seismic systems have been developed in recent years for passive control of the structures. Buckling restrained brace (BRB) (Fig. 1) is among the common systems which can provide stable hysteretic energy damping, as well as symmetric ductile

∗Corresponding author, Assistant Professor
E-mail: Darvishan@riau.ac.ir
[a]MSc. Graduate
E-mail: veysmoradi@alumni.iust.ac.ir

Copyright © 2018 Techno-Press, Ltd.

ISSN: 2092-7614 (Print), 2092-7622 (Online)

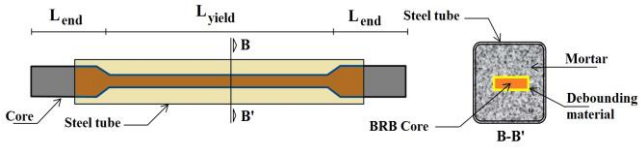

Fig. 1 A typical BRB brace

behavior on both tension and compression demands. As compared to regular concentric bracing systems, BRBs are quite an improvement (Khorami *et al*. 2017); albeit their limited restoring force after brace yielding might still pose some problems and inevitably increase the risk of large inelastic drift concentration which could result on formation of soft-story mechanism on some story levels (Ariyaratana *et al*. 2011). Such an effect could be even worse in near-fault seismic zones where structures might experience strong pulse-like record. To tackle such an issue, several measures could be implemented to improve the performance of BRBs against soft-story mechanism such as improving brace connection details (Fahnestock *et al*. 2007, Richards and Miller 2014) or using dual systems (e.g., Ariyaratana and Fahnestock 2011, Richards and Miller 2014). Recently, it has been suggested to utilize the mega bracing configuration, in BRB frames, to enhance their damage distribution capabilities and preclude the formation of soft stories. Due to the special arrangement of diagonal braces in mega-bracing configuration, the brace force could transmit from upper stories to bottom one without any influence on the beams (Vafaei and Eskandari 2015); thus engaging the whole frame more uniformly to withstand the seismic force. Despite the fact that utilizing BRBs in mega-bracing frame (MBF) systems tends to be promising, a limited number of recent studies have investigated the utilization of such braces in mega-bracing configuration. To gain more insight about the performance of mega-BRB frames, a probabilistic framework can be utilized for quantifying the seismic reliability of such frames against future random earthquakes. This paper focuses on the probabilistic seismic assessment of BRB frames with mega-bracing configuration. For this purpose, a group of mega-buckling restrained braced frames with different number of stories are considered for nonlinear static (pushover) and incremental dynamic analysis (IDA). Two groups of near-fault seismic ground motions (Pulse-Like and Non-Pulse records) are selected, as recommended by FEMA-P695 (2009), to take into account the record-to-record (RTR) variability, as well as the effects of near-faults' strong velocity pulses on the results. In the next step, a detailed seismic reliability assessment is carried out using two different probabilistic frameworks including IM-based and EDP-based, to gain a better understanding of the structures' seismic behavior.

2. Mega-buckling restrained braced frames

Mega bracing (MB) systems may be utilized as a main lateral resisting structure or with combination of other systems (such as moment resisting frames and tube

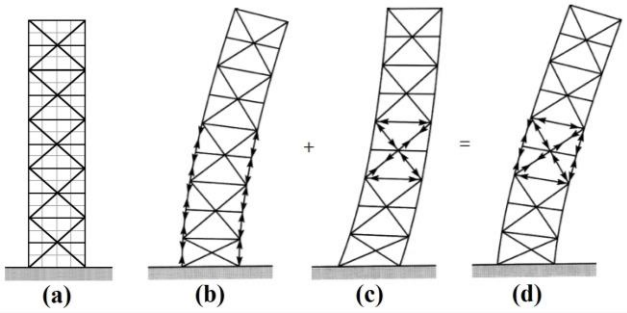

Fig. 2 (a) General mega-braced frame; (b) flexural deformation, (c) shear deformation, and (d) combined configuration (Taranath 2012)

systems), depending on the height of structure and target design requirements. Bracing can be installed within a single bay or span the entire face of the building and tie the whole frame together. This would make the structure similar to a vertical truss as depicted in Fig. 2 (Taranath 2012). The system resists the lateral seismic loads through axial stiffness of the braces and columns. Columns act as the chords in resisting the overturning moment (which is called the flexural deformation), while braces perform as web members by resisting the horizontal shear load (shear deformation). As for the dual brace-tube systems, the diagonals also contribute in carrying the gravity loads as well as decreasing the shear-lag effects (Zahiri-Hashemi *et al*. 2013). Mega bracing pattern has been utilized in some of the important super-tall buildings such as Bank of China (in Hong Kong) and John Hancock building (in Chicago).

Due to the optimal bracing layout of MB systems, they are capable of providing high level of stiffness which plays a decisive role in design of the tall buildings. In fact, it has been shown by Yu *et al*. (2015) that for a 4-bay 4-story frame, the lateral stiffness of a mega X bracing pattern leads to be the stiffest four-bay 4-story frame among the total of 4^4=256 possible symmetric arrangements (4 different case for each story). Although their research was limited to 4-story buildings only, it can be deduced that mega-bracing arrangement could also lead to an optimal braced layout with high stiffness for buildings with more stories, as taller frames can be considered as a number of smaller frames connected to each other.

Considering the beneficial characteristics of BRBs over regular braces, it is believed that utilizing BRBs with mega-bracing arrangement would result in an economized design which utilizes the brace's ductility as well as an effective bracing arrangement with high stiffness. Despite the fact that utilizing BRBs in mega-bracing frame (MBF) systems tends to be promising, the number of studies that have investigated the utilization of such braces in mega-bracing configuration is limited. Among the researches relevant to this paper are the studies by Sarno and Elnashai (2009) who compared the efficiency of CBF and mega-X-braced retrofitting. The results showed the superior performance of the later with 50% reduction in lateral drift. By investigating the seismic performance of high-rise tubular frames with exterior bracing, Kim *et al*. (2009) found that utilizing BRBs instead of CBFs could dramatically enhance

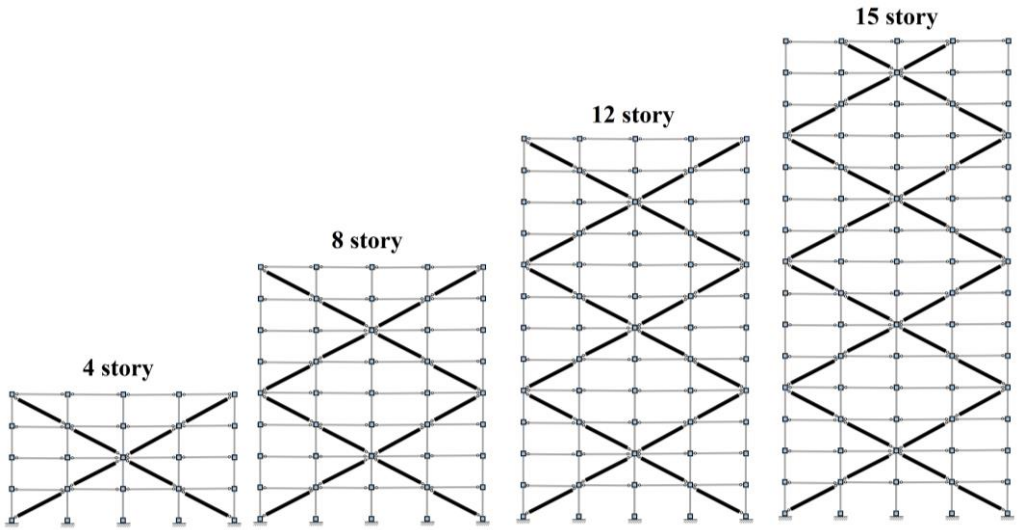

Fig. 3 Brace configuration of the modelled structures

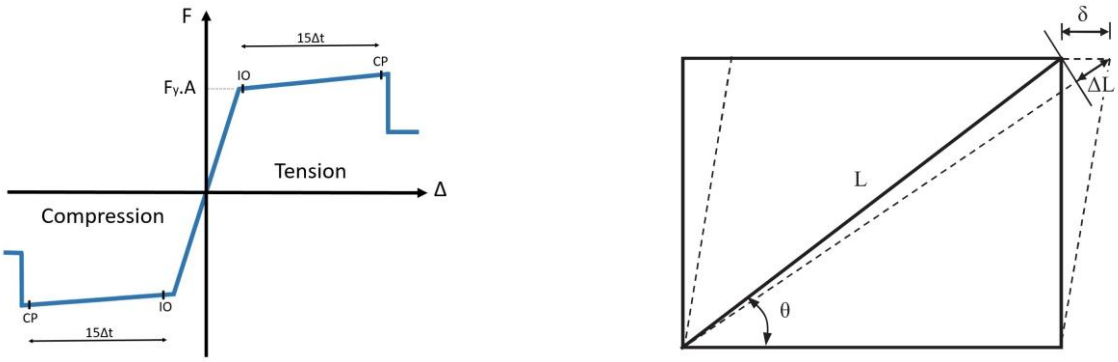

Fig. 4 (a) Force-deformation relation for the BRBs and (b) Correlation of BRB deformation and associated story drift

the structural safety against large earthquake. Sheikh and Masoumi (2014) analyzed the effect of brace configuration in seismic performance of tall steel frames with ordinary braces. Their result indicated a better seismic energy absorption for mega-bracing as compared to other cases. Vafaei and Eskandari (2014) investigated the performance of mega-BRBF using nonlinear time-history analyses and noted the more concentration of story drifts in lower stories. By adding rigid trusses to the outside of a common BRB, Guo *et al*. (2017) experimentally tested a modified BRB brace with improved external restraining flexural stiffness and load-carrying capacity for long-span bracing of mega-structures.

3. Structural characteristics

To study the performance of mega-BRB frames, four different frames (4, 8, 12 and 15 stories) designed by Vafaei and Eskandari (2015) are considered for analysis. Frames are considered to be located in a seismic site with distance less than 5 km to an active fault. Structures are designed based on AISC 341-05 (AISC 2005) and recommendations of Steel TIPS-07 (López and Sabelli, 2004). Near-fault provisions of UBC97 (UBC 1997) are used for seismic design. Dead and live loads are 4.7 KN/m² and 2 KN/m² for floors, and 4 KN/m² and 1.5 KN/m² for roof floor, respectively. Equivalent lateral force method is used for design of the structures. The response modification factor of R=7 and deflection amplification factor of C_d=5.5 were considered for design. The buildings have two mega-bracing configuration in X direction of plan perimeter; while moment resisting system withstand the lateral loads in Y direction. The plan is symmetrical (Fig. 5) with span length of 6.0 m and story height equal to 3.2 m; therefore, 2D frame models could be implemented for analysis (Fig. 3). Further details corresponding to the building design including frame members can be found in (Vafaei and Eskandari 2015).

Nonlinear modelling of the frames was conducted using OpenSEES software package (Mazzoni *et al*. 2006). Distributed plasticity approach with 60 fibers were utilized for beam and column modelling. Steel01 material with yield stress=350 MPa was selected for beam and columns with strain hardening ratio of 2%. To include nonlinear buckling of columns, an initial imperfection up to 1/1000 were considered in mid-spans. Damping coefficient of 5% were designated for the nonlinear analysis. For BRB modelling, corotational truss element were utilized with Giuffre-Menegotto-Pinto steel material (Steel02) which can take into account the strain-hardening effects (Veismoradi *et al*. 2016). The yield stress for BRBs were assumed to be 290

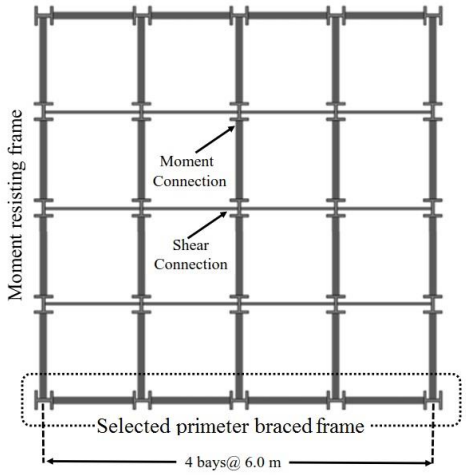

Fig. 5 Plan view of the selected structures

MPa and the maximum ductility of 15 were considered for BRB braces in inelastic behavior, by utilizing MinMax material (Asgarian and Shokrgozar 2009) (Fig. 4(a)). It is worth noting that for the modelled structures, BRB mega-bracing is the only system to withstand lateral loads, thus the brace deformation (ΔL) can be simply correlated to a story drift, δ (Fig. 4(b)). The associated threshold drifts for the performance levels of immediate occupancy (IO) and collapse prevention (CP) were calculated as 0.4% and 4.1%, respectively.

To adequately address the hysteresis behavior of the braces in numerical modeling, calibration is carried out. The isotropic parameters of Steel02 (i.e., a1, a2, a3 and a4) were calibrated using specimen No. 99-1 from PEER Report 2002/08 (Black *et al.* 2002). It is worth noting that two loading protocol were considered for verification: SAC basic loading protocol and SAC near-field loading protocol, to consider the BRB behavior for both Non-pulse and Pulse-like ground motions. The hysteretic results of the analytical brace models are illustrated in Fig. 6. The obtained first three elastic modes of the frames calculated from eigenvalue analysis are presented in Table 1.

Table 1 Calculated fundamental periods for the frames

Mega-braced frames	Mode 1	Mode 2	Mode 3
4-story	0.532	0.238	0.163
8-story	0.772	0.309	0.211
12-story	1.088	0.410	0.262
15-story	1.302	0.476	0.292

4. Pushover assessment

For seismic assessment of the structures, first a pushover analysis is conducted. Pushover is a simple and effective nonlinear analysis tool which is suggested by several building codes and can provide adequate information about nonlinear behavior of structures from elastic range to near collapse. To perform pushover analysis, initially an eigen analysis is carried out to find the dominant period and mode shapes of the structures. Then, a pushover analysis is conducted by lateral progressive load pattern similar to the first mode shape.

As can be seen from Fig. 7, Lateral stiffness of mega-BRB frames decreases by increase in height of the structure. However, the stiffness variations are not tangible. Also, the frames exhibit a similar trend in post-elastic region as the

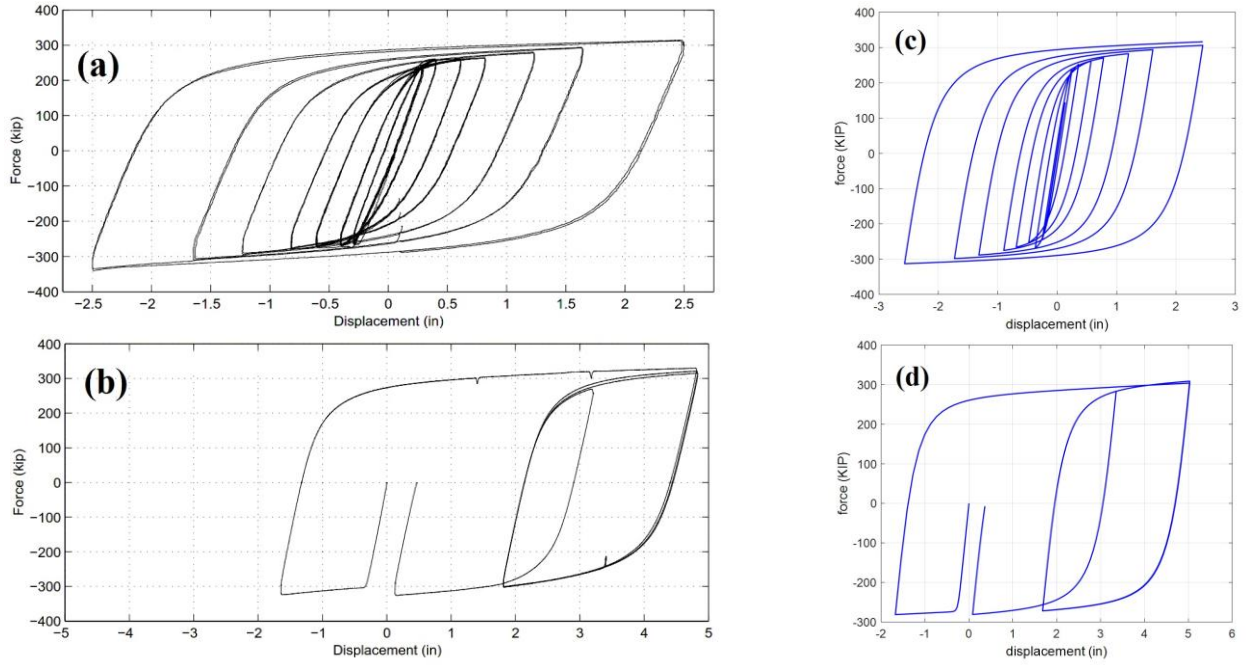

Fig. 6 Calibration of Steel02 material using experimental data from PEER Report (Black *et al*. 2002). BRB brace subjected to two sets of loading protocol: SAC basic loading protocol (a), SAC near-field loading protocol (b) and the calibrated numerical models, (c) and (d)

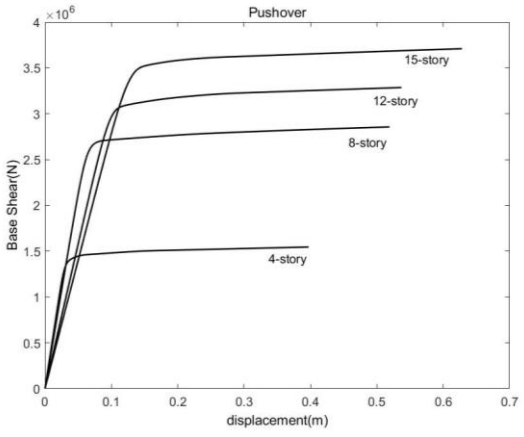

Fig. 7 Nonlinear pushover analysis of Mega-BRB frames

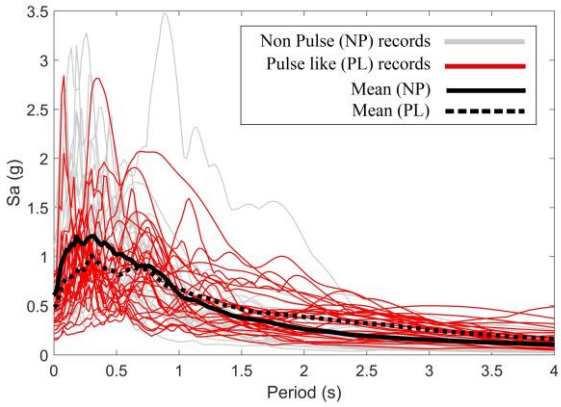

Fig. 8 Spectral plot for the both record sets

slope of pushover curves are approximately the same. In total, frames show desirable ductility. Also, low post-yield stiffness in BRBs is compensated by high lateral stiffness and large base shears in mega bracing configuration.

5. Incremental dynamic analysis

Incremental dynamic analysis (IDA) is a widely used analysis method to investigate the seismic behavior of structures more thoroughly (Vamvatsikos and Cornell 2002). This technique includes a series of nonlinear dynamic analysis using an ensemble of seismic ground motion with multiple scale factors to cover a whole dynamic performance of the frames from elastic region to complete structural collapse. To conduct the IDA, a sufficient number of records are required to consider record-to-record (RTR) variability. It is also preferred that records would not be dependent on hazard deaggregation properties and building-specific properties of the structure such as structural period (FEMA 2009). Here, we used 28

Table 2 Selected ground motion records for analysis

Near-Fault Pulse-Like Records							
No.	Mw	Year	Eq. Name	Station	NEHRP Class	V_{S30} (m/s^2)	Fault Type
1	6.5	1979	Imperial Valley-06	El Centro Array #6	D	203	Strike-slip
2	6.5	1979	Imperial Valley-06	El Centro Array #7	D	211	Strike-slip
3	6.9	1980	Irpinia, Italy-01	Sturno	B	1000	Normal
4	6.5	1987	Superstition Hills-02	Parachute Test Site	D	349	Strike-slip
5	6.9	1989	Loma Prieta	Saratoga - Aloha	C	371	Strike-slip
6	6.7	1992	Erzican, Turkey	Erzincan	D	275	Strike-slip
7	7.0	1992	Cape Mendocino	Petrolia	C	713	Thrust
8	7.3	1992	Landers	Lucerne	C	685	Strike-slip
9	6.7	1994	Northridge-01	Rinaldi Receiving Sta	D	282	Thrust
10	6.7	1994	Northridge-01	Sylmar - Olive View	C	441	Thrust
11	7.5	1999	Kocaeli, Turkey	Izmit	B	811	Strike-slip
12	7.6	1999	Chi-Chi, Taiwan	TCU065	D	306	Thrust
13	7.6	1999	Chi-Chi, Taiwan	TCU102	C	714	Thrust
14	7.1	1999	Duzce, Turkey	Duzce	D	276	Strike-slip
15	6.8	1976	Gazli, USSR	Karakyr	C	660	Thrust
16	6.5	1979	Imperial Valley-06	Bonds Corner	D	223	Strike-slip
17	6.5	1979	Imperial Valley-06	Chihuahua	D	275	Strike-slip
18	6.8	1985	Nahanni, Canada	Site 1	C	660	Thrust
19	6.8	1985	Nahanni, Canada	Site 2	C	660	Thrust
20	6.9	1989	Loma Prieta	BRAN	C	376	Strike-slip
21	6.9	1989	Loma Prieta	Corralitos	C	462	Strike-slip
22	7.0	1992	Cape Mendocino	Cape Mendocino	C	514	Thrust
23	6.7	1994	Northridge-01	LA - Sepulveda VA	C	380	Thrust
24	6.7	1994	Northridge-01	Northridge - Saticoy	D	281	Thrust
25	7.5	1999	Kocaeli, Turkey	Yarimca	D	297	Strike-slip
26	7.6	1999	Chi-Chi, Taiwan	TCU067	C	434	Thrust
27	7.6	1999	Chi-Chi, Taiwan	TCU084	C	553	Thrust
28	7.9	2002	Denali, Alaska	TAPS Pump Sta. #10	C	553	Strike-slip

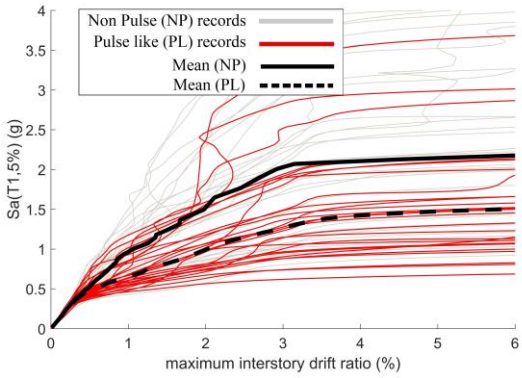

Fig. 9 Multi-IDA curves for the 4-story frame

pair of near-fault earthquakes (56 individual components in total) recommended by FEMA-P695 (2009) (Table 2).

It is worth mentioning that the first fourteen records include strong velocity pulses, while the second fourteen records are non-pulse ground motion, as judged by wavelet analysis method proposed by baker (2007). These ground motions meet the "large number of records" objective which means that the number of records are 'statistically' sufficient for seismic assessment. Records are applicable to a wide range of structural systems with different sites such as sites with different ground motion hazard functions, site and source conditions.

Fig. 8 compares the acceleration spectra for both records subsets and Fig. 9 compares the IDA curves for the 4-story mega-brace frame, using both seismic records.

Fig. 10 summarizes the 50% fractiles for the both records subset. As can be seen, spectral acceleration of the

Table 3 50% summarized capacities for the structures

Selected frames	Non-pulse ground motions						Pulse-like ground motions					
	S_a			$\theta_{\max(\%)}$			S_a			$\theta_{\max(\%)}$		
	IO	CP	GI	IO	CP	GI	IO	CP	GI	IO	CP	GI
4 story	0.44	2.05	2.20	0.40	3.20	$+\infty$	0.42	1.42	1.05	0.40	3.10	$+\infty$
8 story	0.40	2.11	2.15	0.40	4.10	$+\infty$	0.37	1.40	1.48	0.40	4.10	$+\infty$
12 story	0.24	1.27	1.30	0.40	4.10	$+\infty$	0.24	0.85	0.95	0.40	4.10	$+\infty$
15 story	0.19	1.04	1.09	0.40	4.10	$+\infty$	0.21	0.97	1.03	0.40	4.10	$+\infty$

structures is decreased under pulse-like ground motions. This is more obvious for shorter buildings, as far as 15 story structure exhibits approximately similar behavior for both record sets. However, it is notable that drift values near collapse of the structures are approximately the same for both cases which indicates that the ultimate drift capacity of the structures do not differ in pulse-like and non-pulse earthquakes.

To quantify IDAs, summarized capacities are tabulated in Table 3. According to the table, existence of pulse in ground motion records has led to decrease in spectral acceleration capacities, especially for shorter buildings. This is more tangible for CP limit state. Unlike the Sa capacities, Max IDRs (θ_{max}) are not influenced by pulse-like earthquakes, since θ_{max} are almost the same for both cases for the assumed performance levels.

6. IM-based performance assessment

In the following sections, seismic behavior of the structures is investigated more thoroughly in the context of

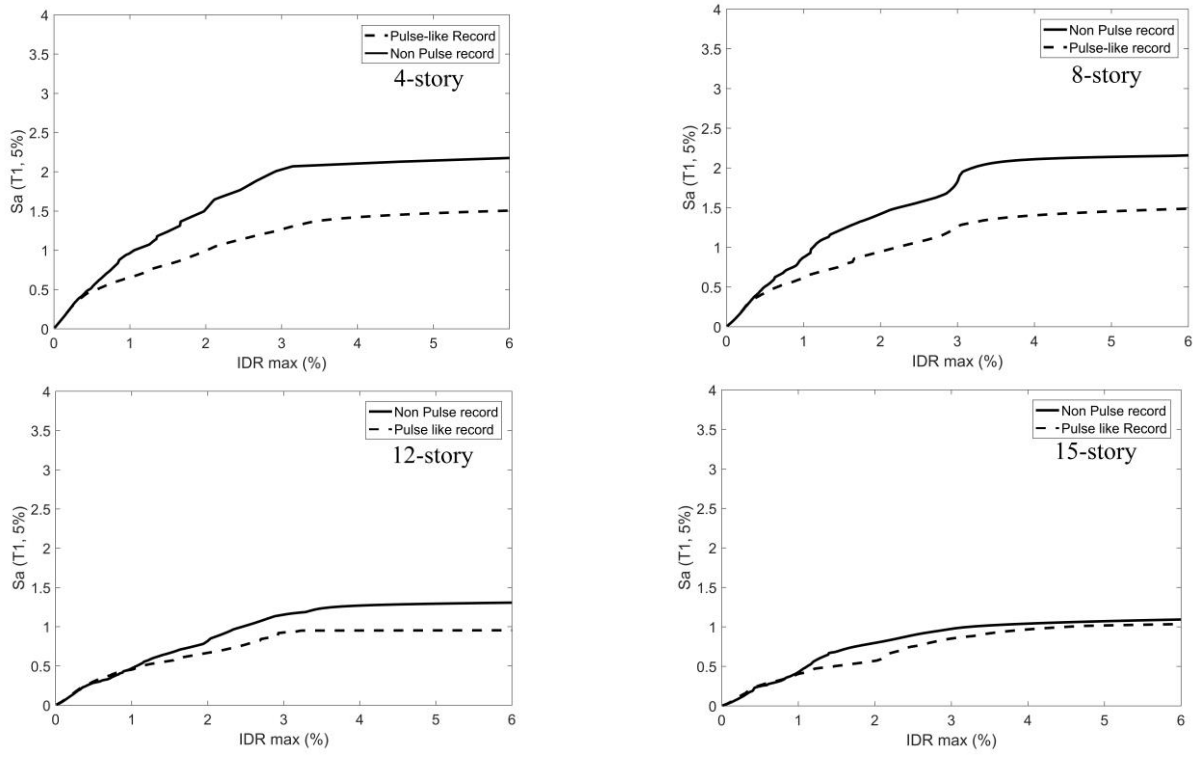

Fig. 10 Comparison of mean IDA curves for both record sets

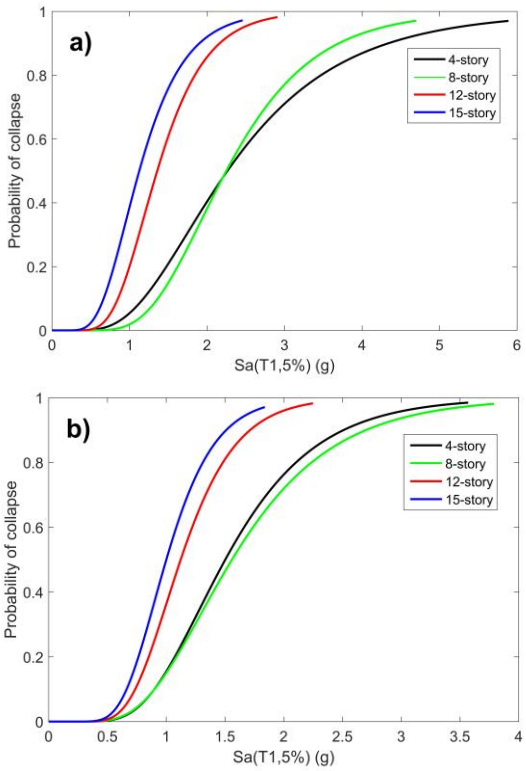

Fig. 11 collapse fragility curves for (a) non-pulse records and (b) pulse-like records

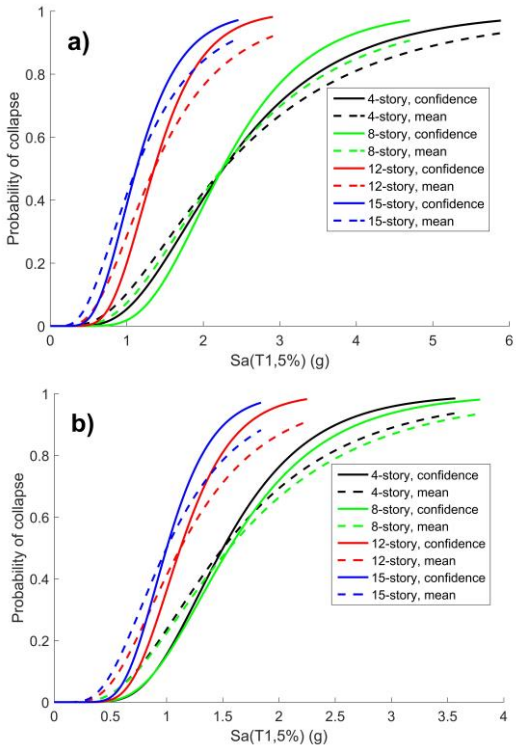

Fig. 12 effects of epistemic uncertainties on the collapse fragility curves for (a) non-pulse records and (b) pulse-like records

performance based earthquake engineering (PBEE). Two well-known frameworks are utilized for seismic risk assessments of mega-BRB frames: the IM-based framework presented by Zareian *et al*. (2010) and SAC/FEMA format (Jalayer and Cornell 2003). In both of these frameworks, sources of uncertainty are categorized to *aleatory* and *epistemic* which are assumed to be independent. Aleatory uncertainties (type I) origin from record to record variabilities and unknown characteristics of future earthquakes. Epistemic uncertainties (type II) are rooted in limited knowledge in numerical modeling and construction variabilities which indicates that ground motions and structural models used for analysis are only an estimates of real values. To account for such an uncertainty, both procedures, employ lognormal distribution for the uncertain variables and median estimates and their associated dispersion are used for probabilistic analyses. However, the main difference between the two frameworks is that they use different parameters for demand/capacity representation. SAC/FEMA procedure is an 'EDP-based' method which employs engineering demand parameter (EDP) for collapse potential assessment, while the 'IM-based' method directly employs ground motion intensity measure (IM). Both procedures use three variables including ground motion intensity, seismic demand, and seismic capacity to account uncertainty. However, they differ in the way that they combine these uncertain variables. The aim of IM-based procedure is to address collapse at a desired hazard level while EDP-based stipulates that the mean annual frequency (MAF) of the structure at collapse level be limited to less than 2%/50 yr. The IM-based method is utilized here, while the EDP-based method is investigated in next section.

6.1 Fragility curves

Fragility analysis is a common tool to represent the safety of structures against collapse. In other words, Fragility curve is a measure that denotes the probability of exceeding a desired performance level as a function of intensity measure. Zareian *et al*. (2010) introduced collapse fragility for the damage state that the structure experiences global dynamic instability. By definition, the fragility takes the following mathematical form

$$P\left[C \middle| IM = im_i\right] = P\left[IM_C < IM = im_i\right] \quad (1)$$

If we only consider the aleatory uncertainties, assuming the spectral acceleration, S_a, as the intensity measure, the probability of collapse as per the hazard level P_R (or intensity level, S_a^{PR}), would be

$$P\left(C \middle| Sa^{P_R}\right) = \Phi\left(\frac{Ln\left(Sa^{P_R}\right) - Ln\left(\eta_c\right)}{\beta_{RC}}\right) \quad (2)$$

Where $\Phi(\ )$ denotes the standard normal distribution function, and η_c and β_{RC} are median and dispersion of capacity due to ground motion variability. This form of fragility representation is very popular in seismic engineering and has widely utilized in many investigations. However, it does not consider epistemic uncertainties. Fig. 11 shows fragility plots of the buildings for both earthquake

record subsets. It is clear that 4- and 8- story frames exhibit similar probability of exceeding. However, larger structures (i.e. 12 and 15- story structures) show considerably higher probabilities of exceedance. In general, safety of structures against collapse decreases by increase in height of the structures. Also, existence of pulse in ground motions causes higher level of hazard for all of the structures compared to non-pulse ones.

For a more realistic representation of fragility, epistemic uncertainties must be included. It is assumed that the median estimate of the fragility curve is again a variable parameter with median, η_c, and dispersion, β_{RC}. Two options exist to combine variability in IM-based probabilistic calculations: 'confidence level' and 'mean' method. As its name implies, the confidence level method states the probability of exceeding by Y confidence.

$$P_Y\left[C\middle|Sa^{P_R}\right]=\Phi\left(\frac{Ln\left(Sa^{P_R}\right)-Ln\left(\eta_C^Y\right)}{\beta_{RC}}\right)$$
$$\eta_C^Y=\hat{\eta}_C e^{-\beta_{UC}K_Y} \quad (3)$$

K_Y is the standard Gaussian variable corresponding to probability Y. The mean method employs the integration of both aleatory and epistemic uncertainties, $\beta_{TC}=\sqrt{\beta_{RC}{}^2+\beta_{UC}{}^2}$, for calculation of lognormal distribution as

$$P\left(C\middle|Sa^{P_R}\right)=\Phi\left(\frac{Ln\left(Sa^{P_R}\right)-Ln\left(\hat{\eta}_c\right)}{\beta_{TC}}\right) \quad (4)$$

Fig. 12 compares the results of fragility curves of the two procedures. Probabilities of confidence-level method are plotted for 50% confidence. According to the figure, for large level of spectral accelerations, confidence level method yields larger probabilities of exceedance while for smaller spectral accelerations it yields lower probability of exceedance. However, both procedures show similar trends and their difference is not sensible. It is worth to note that for larger confidence levels (for instance, Y=84%), confidence-level method yields much larger probability of exceedance than the mean method.

6.2 Mean annual frequency of exceeding IM

Seismologists traditionally use seismic hazard, $\lambda_{Sa}(Sa)$, to quantify probability of exceeding a ground intensity measure. Like the hazard curve which shows the ground hazard, a structure-specific hazard can be defined as the probability of exceeding a IM value. For collapse performance level (Zareian *et al*. 2010)

$$\lambda_C=\int_{all\ IM}P\left(C\middle|IM\right)\left|d\lambda_{Sa}\left(IM\right)\right. \quad (5)$$

Where λ_{Sa} is the hazard curve. To yield the closed-form relationship for the above Equation, some simplifications are needed. First, hazard curve is to be approximated by a power-law:

$$\bar{\lambda}_{Sa}(Sa)=P[S_a\geq s_a]=k_0Sa^{-k} \quad (6)$$

Where k and k_0 are constant regression coefficients. In addition, a power relationship can be fitted to correlate

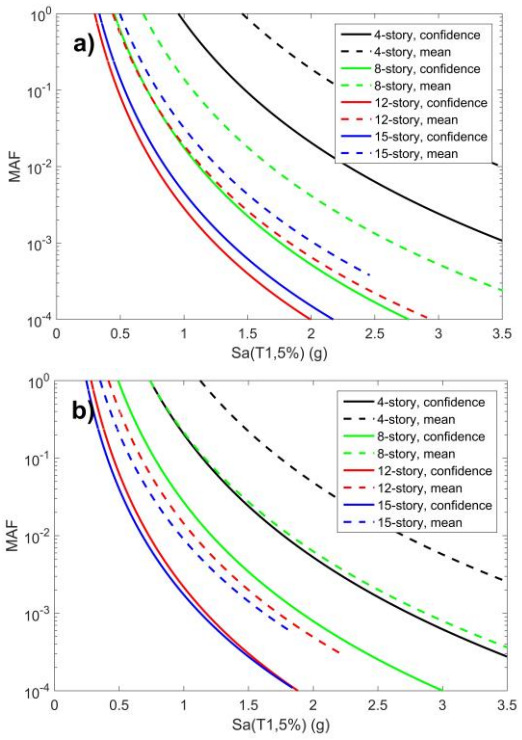

Fig. 13 The calculated MAF for (a) non-pulse records and (b) pulse-like records

median EDP, $E\hat{D}P$, (here maximum interstory drift ratio, EDP_d) to spectral acceleration, S_a, at least in the vicinity of the desired limit state.

$$E\hat{D}P_d=a(S_a)^b \quad (7)$$

Where a and b are constant coefficients. Now, the closed-form equation to estimate MAF can be derived

$$\lambda_C=\lambda_{Sa}\left(\eta_C\right)\left[\exp\left(\frac{1}{2}k^2\beta_{RC}^2\right)\right] \quad (8)$$

Eq. (8) only accounts aleatory uncertainties. Again, to include epistemic uncertainty two approaches exist. The closed-form equation based on confidence method is shown in Eq. (9)

$$\lambda_C^Y=\int_{all\ IM}P_Y\left(C\middle|IM\right)\left|d\bar{\lambda}_{Sa}\left(IM\right)\right.$$
$$\lambda_C^Y=\bar{\lambda}_{Sa}\left(\hat{\eta}_C\right)\left[\exp\left(\frac{1}{2}k^2\beta_{RC}^2\right)\right]\left[\exp\left[K_Y\left(k\beta_{UC}\right)\right]\right] \quad (9)$$

β_{UC} is the epistemic uncertainty due to variability in structural modelling. In this paper, β_{UC}=0.4 is adopted as suggested by Zareian and Krawinkler (2007).

Mean method uses total capacity dispersion, β_{TC}, for calculation of collapse MAF

$$\bar{\lambda}_C=\int_{all\ IM}P_Y\left(C\middle|IM\right)\left|d\bar{\lambda}_{Sa}\left(IM\right)\right.$$
$$\lambda_C^Y=\bar{\lambda}_{Sa}\left(\hat{\eta}_C\right)\left[\exp\left(\frac{1}{2}k^2\beta_{TC}^2\right)\right] \quad (10)$$

Fig. 13 illustrates the MAF of IM-based methods. From

Table 4 Collapse confidence levels for different hazard levels

structure	hazard	k	b	β_{RC}	β_{RD}	β_{UD}	β_{UC}	$C.L.^{84\%}$	$C.L.^{50\%}$	$C.L.^{mean}$
Non-pulse ground motions										
4-story	50%/50	5.27	1.15	0.37	0.58	0.11	0.40	0.93	0.96	0.94
	2%50	5.27	1.15	0.37	0.58	0.11	0.40	0.93	0.99	0.94
8-story	50%/50	5.09	1.19	0.10	0.35	0.67	0.40	0.92	0.98	0.96
	2%50	5.09	1.19	0.10	0.35	0.67	0.40	0.98	1.00	0.98
12-story	50%/50	4.86	1.20	0.12	0.46	0.09	0.40	0.94	1.00	0.94
	2%50	4.86	1.20	0.12	0.46	0.09	0.40	0.98	0.99	0.99
15-story	50%/50	4.93	1.04	0.10	0.39	0.07	0.40	0.93	0.99	0.95
	2%50	4.93	1.04	0.10	0.39	0.07	0.40	0.98	1.00	0.98
Pulse-like ground motions										
4-story	50%/50	5.27	1.94	0.09	0.45	0.08	0.40	0.90	0.98	0.90
	2%50	5.27	1.94	0.09	0.45	0.08	0.40	0.97	1.00	0.97
8-story	50%/50	5.09	1.72	0.11	0.54	0.10	0.40	0.94	0.98	0.94
	2%50	5.09	1.72	0.11	0.54	0.10	0.40	0.97	1.00	0.97
12-story	50%/50	4.86	1.68	0.165	0.36	0.07	0.40	0.95	0.99	0.95
	2%50	4.86	1.68	0.165	0.36	0.07	0.40	0.99	1.00	0.99
15-story	50%/50	4.93	1.43	0.11	0.37	0.06	0.40	0.97	0.99	0.97
	2%50	4.93	1.43	0.11	0.37	0.06	0.40	0.99	0.99	0.99

the figure it is obvious that shorter structures experience higher values of MAF. This happens as a result of higher spectral acceleration in seismic hazard curves of the structures. However, unlike the fragility curves, MAF of 4- and 8- story structures show the most difference while the MAF of 12- and 15-story frames do not differ a lot. Again, this is due to the inclusion of seismic hazard curve. Seismic hazard curves of shorter stories show much larger MAFs for a specific spectral acceleration level. Moreover, structures under pulse-like ground motions show higher MAFs for all cases, as expected.

6.3 Confidence level

The final product of PBEE calculations is confidence level of the structure against a specific performance level. In confidence level approach, probability, Y, that the median performance level variable, $\hat{\eta}_{PL}$,exceeds η_{PL}^{Y} denotes the confidence level, K_y (Zareian and Krawinkler 2007)

$$\eta_{L.S}^{Y} = \hat{\eta}_{L.S} e^{-\beta_{UC} K_Y} \tag{11}$$

Eq. (11) can be re-written in the form of

$$P_Y(L.S \,|\, Sa^{(P_R)}) = \Phi\left(\frac{Ln(Sa^{(P_R)}) - Ln(\eta_C^Y)}{\beta_{RC}}\right) \tag{12}$$

or

$$\mathrm{C.L^{Y}} = 1 - \Phi\left(\frac{\mathrm{Ln}\left(\mathrm{Sa^{P_R}}\right) - \mathrm{Ln}\left(\eta_{\mathrm{C}}^{\mathrm{Y}}\right)}{\beta_{\mathrm{RC}}}\right) \tag{13}$$

Unlike the confidence method, mean method do not change the median estimate, $\hat{\eta}_C$. Instead, it inflates the dispersion in terms of β_{TC}

$$P_Y(L.S \,|\, Sa^{(P_R)}) = \Phi\left(\frac{Ln(Sa^{(P_R)}) - Ln(\hat{\eta}_C)}{\beta_{TC}}\right) \tag{14}$$

Therefore, the confidence level, Y, would be

$$Y = 1 - \Phi\left(\frac{Ln(Sa^{(P_R)}) - Ln(\hat{\eta}_C)}{\frac{\beta_{UC}.\beta_{TC}}{\beta_{TC} - \beta_{RC}}}\right) \tag{15}$$

Table 4 lists the calculated confidence level (C.L.) values based on IM-based procedure. Two levels of confidence are considered for confidence level method including 50% and 84%. It is observed that confidence level method and mean method yield similar results for Y=84%. However, for Y=50%, confidence level method slightly overestimates C.L. values (up to 12%). b values for pulse-like earthquakes are considerably larger than non-pulse ones (from 37 to 68%) which shows that the slope of IDAs in this case are lower. Also, β_{RC} values show no regular trend. They vary from 0.09 in pulse-like case to 0.37 for non-pulse one. Generally, all of the C.L. values are over 90% which means that all the structures could successfully tolerate the desired performance levels.

7. EDP-based performance assessment

7.1 Mean annual frequency of exceeding EDP

As mentioned in the previous section, in contrast to IM-based approach, EDP-based framework uses engineering demand parameter (EDP) as demand/capacity parameter. One of the main objectives of EDP-based approach is to calculate MAF of a specific performance level. MAF of a performance level incorporates the uncertainty in seismic hazard and structural response. In EDP-based approaches, MAF is defined as conditional probability of exceeding a drift value, EDP_d, or, in brief, drift hazard (Jalayer and Cornell 2003)

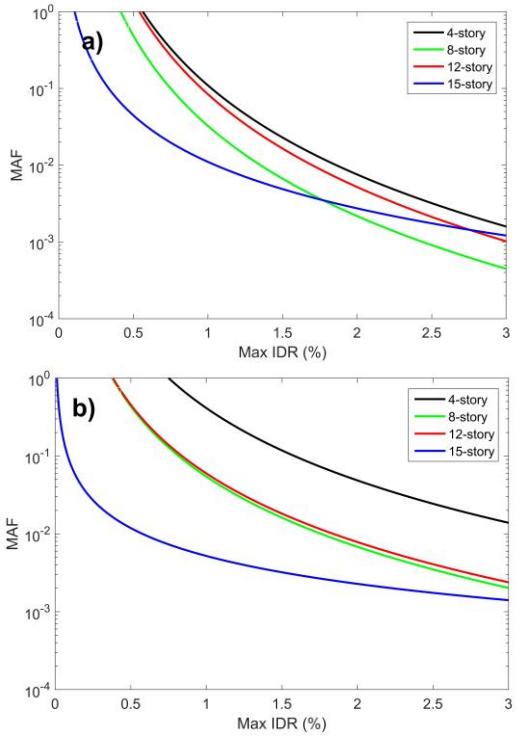

Fig. 14 The calculated drift hazard for (a) non-pulse records and (b) pulse-like records

$$\lambda_D = P\left[EDP_D > EDP_d\right] = \sum P\left[EDP_D > EDP_d\right].P\left[IM = im_i\right] \quad (16)$$

$P[IM=im_i]$ can be found from hazard curve. Considering EDP, IM and λ_D as uncertain variables, and some re-arrangements, the median drift hazard would be

$$\bar{\lambda}_D = \hat{\lambda}_D(Sa^{edp})\left[\exp\left(\frac{1}{2}\frac{k^2}{b^2}\beta_{RD}^2\right)\right]\left[\exp\left(\frac{1}{2}\frac{k^2}{b^2}\beta_{UD}^2\right)\right] \quad (17)$$

Where β_{RD} is dispersion due to record-to-record variability and β_{UD} is dispersion of EDP due to finite number of ground motion records. Fig. 14 depicts the drift hazard for the structures. As usual, shorter structures show higher probabilities of exceedance. Albeit, non-pulse and pulse-like cases show very different behavior. In non-pulse case, 4- and 8- story frames show similar curves while in pulse-like case 8- and 12- story curves are alike. In addition, difference in MAFs for different structures is much tangible in pulse-like case. This is due to larger dispersion in β_{RD}, β_{RC} and b values which means that pulse in ground motion can cause variable response of the structures and also can intensify structural response.

7.2 Confidence level

Among the major class of EDP-based formulations provided for confidence calculations, DCFD format is adopted here since it is the best alternative to the widely-known LRFD format. Limit state frequency is defined as the mean annual rate that demand, EDP_d, exceeds capacity, EDP_C (Jalayer and Cornell 2003)

$$P_{PL} = P\left[EDP_D > EDP_C\right] \quad (18)$$

$$\hat{P}_{PL} = \bar{\lambda}_{Sa}\left[\exp\left(\frac{1}{2}\frac{k^2}{b^2}\beta_{RD}^2\right)\right]\left[\exp\left(\frac{1}{2}\frac{k^2}{b^2}\beta_{RC}^2\right)\right] \quad (19)$$

However, limit state frequency, P_{PL}, is itself an uncertain variable. So a confidence level can be defined around its median:

$$P_{PL}^x = \hat{P}_{PL}\exp[K_x\beta_{P_{PL}}] \quad (20)$$

Where K_x is the standard Gaussian variable and β_{PL} is

$$\beta_{PL} = \sqrt{\left(k^2/b^2\right)\left(\beta_{UD}^2 + \beta_{UC}^2\right)} \quad (21)$$

By definition of

$$\phi = \exp\left[-\frac{1}{2}\frac{k}{b}\left(\beta_{RC}^2 + \beta_{UC}^2\right)\right] \quad (22)$$

$$\gamma = \exp\left[\frac{1}{2}\frac{k}{b}\left(\beta_{RD}^2 + \beta_{UD}^2\right)\right] \quad (23)$$

$$\lambda_x = e^{-\beta_{UT}\left(K_x - \frac{1}{2}\frac{k}{b}\beta_{UT}\right)} \quad (24)$$

Eq. (20) can be re-written as a LRFD like format called DCFD

$$\varphi\hat{EDP}_C.\lambda_x \geq \gamma\hat{EDP}_D \quad (25)$$

or

$$K_x = [-\ln(\lambda_x) + \frac{1}{2}\frac{k}{b}\beta_{UT}^2]/\beta_{UT} \quad (26)$$

Where F.D. is factored demand and F.C. is factored capacity. Table 5 lists the summary of DCFD calculations for 50%/50 and 2%/50 hazard levels. For 50%/50, the difference for Non-pulse and pulse-like earthquakes is not sensible. Since values of b and β_{UD} are very similar for this hazard level, factored demands are almost the same. Therefore, similar confidence levels are obtained. However, large dispersion of FD/FC is observed for 2%/50 case. b values are larger for pulse-like earthquakes which represents lower IDA slopes for CP level. Also, larger record-to-record variability, β_{RD}, is observed for pulse-like earthquakes records. In general, structures showed a desired behavior even for pulse-like earthquakes since they showed about 100% confidence level.

8. Conclusions

Mega-buckling restrained braces are efficient lateral system, capable of providing sufficient lateral stiffness and ductility which are suitable for high-rise buildings. In this study, seismic performance of BRB frames with mega-bracing configuration was investigated. First, the nonlinear pushover analysis was conducted which highlights the high elastic stiffness of the frames with small stiffness variations, along with large inelastic deformation capacity. The

Table-5 Calculated confidence parameters for the frames

		b	β_{RD}	β_{UD}	β_{RC}	β_{UC}	β_{UT}	γ	ϕ	D	C	FD/FC	$C.L.$
Non-pulse ground motions													
4-story	50%/50yr	0.93	0.03	0.01	0.00	0.00	0.20	1.00	0.93	0.17	0.50	0.37	1.00
	2%/50yr	1.22	0.38	0.07	0.36	0.20	0.21	1.22	0.89	0.69	3.17	0.34	1.00
8-story	50%/50yr	0.84	0.11	0.02	0.00	0.20	0.20	1.02	0.92	0.21	0.50	0.46	1.00
	2%/50yr	0.90	0.28	0.05	0.20	0.20	0.21	1.16	0.86	0.76	3.17	0.32	1.00
12-story	50%/50yr	0.83	0.14	0.03	0.00	0.20	0.20	1.04	0.92	0.17	0.50	0.39	1.00
	2%/50yr	1.04	0.32	0.06	0.20	0.20	0.21	1.18	0.88	1.03	3.17	0.43	1.00
15-story	50%/50yr	0.77	0.17	0.03	0.00	0.20	0.20	1.07	0.92	0.20	0.50	0.47	1.00
	2%/50yr	0.55	0.33	0.06	0.20	0.20	0.21	1.41	0.79	0.83	3.17	0.47	1.00
Pulse-like ground motions													
4-story	50%/50yr	1.01	0.06	0.01	0.00	0.20	0.20	1.01	0.94	0.17	0.50	0.37	1.00
	2%/50yr	1.85	0.44	0.08	0.63	0.20	0.22	1.19	0.90	0.15	0.51	0.40	1.00
8-story	50%/50yr	0.84	0.09	0.02	0.00	0.20	0.20	1.02	0.92	0.20	0.50	0.45	1.00
	2%/50yr	2.16	0.28	0.05	0.20	0.20	0.21	1.06	0.94	1.25	3.17	0.45	1.00
12-story	50%/50yr	0.86	0.10	0.02	0.00	0.20	0.20	1.02	0.93	0.17	0.50	0.36	1.00
	2%/50yr	1.26	0.39	0.07	0.20	0.20	0.21	1.22	0.90	1.14	3.17	0.49	1.00
15-story	50%/50yr	0.78	0.12	0.02	0.00	0.20	0.20	1.03	0.92	0.18	0.50	0.39	1.00
	2%/50yr	2.30	0.34	0.06	0.20	0.20	0.21	1.09	0.94	0.86	3.17	0.31	1.00

investigation was continued by IDA analyses and fragility assessment; also, two probabilistic frameworks were employed for seismic reliability assessments for several well-recognized limit states. The PBEE results showed that although conventional fragility analysis is an effective analysis tool, using fragilities which consider both aleatory and epistemic uncertainties can improve the accuracy of the analysis. Nevertheless, MAF of exceeding a performance level may be a more exact parameter than fragility since it employs a combination of seismic hazard and structural response. Also, the results indicated that all the structures exhibit a desired performance in both non-pulse and pulse-like cases, since they show high level of confidence for the designed performance objectives. As a result, it can be concluded that mega-BRB configuration is an effective alternative to conventional BRB bracing systems to withstand near-fault earthquakes.

References

AISC 341-05 (2005), Seismic Provisions for Steel Structural Buildings, American Institute of Steel Construction, Inc., Chicago.

Ariyaratana, C. and Fahnestock, L.A. (2011), "Evaluation of buckling-restrained braced frame seismic performance considering reserve strength", *Eng. Struct.*, **33**(1), 77-89.

Baker, J.W. (2007), "Quantitative classification of near-fault ground motions using wavelet analysis", *Bull. Seismol. Soc. Am.*, **97**(5), 1486-1501.

BC-97 (1997), Uniform Building Code, International Council of Building Officials, USA.

Black, C., Aiken, I.D. and Makris, N. (2002), "Component testing, stability analysis, and characterization of buckling-restrained unbonded braces (TM)", Pacific Earthquake Engineering Research Center.

Di Sarno, L. and Elnashai, A.S. (2009) "Bracing systems for seismic retrofitting of steel frames", *J. Constr. Steel Res.*, **65**(2), 452-465.

Eskandari, R., Vafaei, D., Vafaei, J. and Shemshadian, M.E. (2017), "Nonlinear static and dynamic behavior of reinforced concrete steel-braced frames", *Earthq. Struct.*, **12**(2), 191-200.

Fahnestock, L.A., Ricles, J.M. and Sause, R. (2007), "Experimental evaluation of large-scale buckling-restrained braced frame", *J. Struct. Eng.*, **133**(9), 1205-1214.

FEMA P-695 (2009), Quantification of Building Seismic Performance Factors, Federal Emergency Management Agency.

Guo, Y.L., Zhou, P., Wang, M.Z., Pi, Y.L., Bradford, M.A. and Tong, J.Z. (2017), "Experimental and numerical studies of hysteretic response of triple-truss-confined buckling-restrained braces", *Eng. Struct.*, **148**, 157-174.

Jalayer, F. and Cornell, C.A. (2003), "A technical framework for probability-based demand and capacity factor (DCFD) seismic formats", RMS Technical Rep. No. 43 to the PEER Center, Dept. of Civil and Environmental Engineering, Stanford Univ., Stanford.

Kalkan, E. and Kunnath, S.K. (2006), "Effects of fling step and forward directivity on seismic response of buildings", *Earthq. Spectra*, **22**(2), 367-390.

Khorami, M., Alvansazyazdi, M., Shariati, M., Zandi, Y., Jalali, A. and Tahir, M. (2017), "Seismic performance evaluation of buckling restrained braced frames (BRBF) using incremental nonlinear dynamic analysis method (IDA)", *Earthq. Struct.*, **13**(6), 531-538.

Kim, J., Park, J., Shin, S.W. and Min, K.W. (2009) "Seismic performance of tubular structures with buckling restrained braces", *Struct. Des. Tall Spec. Build.*, **18**(4), 351-370.

López, W.A. and Sabelli, R. (2004), "Seismic design of buckling-restrained braced frames", Steel TIPS 07.2004, Structural Steel Educational Council.

Mazzoni, S., McKenna, F., Scott, M.H. and Fenves, G.L. (2006), "The Open System for Earthquake Engineering Simulation (OpenSEES) user command-language manual".

Mortezaei, A., Ronagh, H.R. and Kheyroddin, A. (2010), "Seismic evaluation of FRP strengthened RC buildings subjected to near-fault ground motions having fling step", *Compos. Struct.*, **92**(5), 1200-1211.

Richards, P.W. and Miller, D.J. (2014), "High-yield-drift steel moment frames", *Proceedings of the 10th U.S. National Conference on Earthquake Engineering*, Anchorage, Alaska.

Sheikh, H. and Massumi, A. (2014) "Effects of bracing configuration on seismic behavior of tall steel structures subjected to earthquake ground motions", *Proceedings of the 10th U.S. National Conference on Earthquake Engineering*, Anchorage, Alaska.

Soleimani Amiri, F., Ghodrati Amiri, G. and Razeghi, H. (2013), "Estimation of seismic demands of steel frames subjected to near-fault earthquakes having forward directivity and comparing with pushover analysis results", *Struct. Des. Tall Spec. Build.*, **22**(13), 975-988.

Stewart, J.P., Chiou, S.J., Bray, J.D., Graves, R.W., Somerville, P.G. and Abrahamson, N.A. (2002), "Ground motion evaluation procedures for performance-based design", *Soil Dyn. Earthq. Eng.*, **22**(9-12), 765-772.

Vafaei, D. and Eskandari, R. (2015), "Seismic response of mega buckling-restrained braces subjected to fling-step and forward-directivity near-fault ground motions", *Struct. Des. Tall Spec. Build.*, **24**(9), 672-686.

Vamvatsikos, D. and Cornell, C.A. (2002), "Incremental dynamic analysis", *Earthq. Eng. Struct. Dyn.*, **31**(3), 491-514.

Veismoradi, S., Amiri, G.G. and Darvishan, E. (2016), "Probabilistic seismic assessment of Buckling Restrained Braces and Yielding Brace Systems", *Int. J. Steel Struct.*, **16**(3), 831-843.

Yu, X., Ji, T. and Zheng, T. (2015), "Relationships between internal forces, bracing patterns and lateral stiffnesses of a simple frame", *Eng. Struct.*, **89**, 147-161.

Zahiri-Hashemi, R., Kheyroddin, A. and Farhadi, B. (2013), "Effective number of mega-bracing, in order to minimize shear lag", *Struct. Eng. Mech.*, **48**(2), 173-193.

Zareian, F. and Krawinkler, H. (2007), "Assessment of probability of collapse and design for collapse safety", *Earthq. Eng. Struct. Dyn.*, **36**(13), 1901-1914.

Zareian, F., Krawinkler, H., Ibarra, L. and Lignos, D. (2010), "Basic concepts and performance measures in prediction of collapse of buildings under earthquake ground motions", *Struct. Des. Tall Spec. Build.*, **19**(1-2), 167-181.

AT